Ultrasound- and microwave-assisted preparation of lead-free palladium catalysts: effects on kinetics of diphenylacetylene semi-hydrogenation

Zhilin Wu[a], Nikolay Cherkasov[b], Emily Borretto[a], Giancarlo Cravotto[a]*, Alex O. Ibhadon[b]*, Jonathan Medlock[c], Werner Bonrath*[c]

[a] Dipartimento di Scienza e Tecnología del Farmaco, Universty of Turin, Via P. Giuria 9, I-10125 Torino, Italy.

[b] Catalysis and Reactor Engineering Research Group, Department of Chemistry and School of Biological, Biomedical and Environmental Sciences, University of Hull, Cottingham Road, Hull HU6 7RX, United Kingdom

[c] DSM Nutritional Products Ltd., Research and Development, P.O. Box 2676, 4002 Basel, Switzerland

* Corresponding authors. E-mail: giancarlo.cravotto@unito.it (G. Cravotto); a.o.ibhadon@hull.ac.uk (A.O. Ibhadon); werner.bonrath@dsm.com (W. Bonrath)

Keywords: semi-hydrogenation, diphenylacetylene, lead-free Pd catalyst, Lindlar catalyst, ultrasound, microwaves.

1

Abstract

The effect of environmentally benign enabling techniques such as ultrasound and microwaves on the preparation of lead-free Pd-catalyst has been studied. A one-pot method of the catalyst preparation using ultrasound dispersing of palladium acetate in the presence of the surfactant/capping agent and boehmite support produced the catalyst containing Pd nanoparticles and reduced the pores larger than 4 nm in the boehmite support. This catalyst demonstrated higher activity and selectivity. The comparison of diphenylacetylene (DPA) hydrogenation kinetic showed that the catalyst obtained in the one-pot procedure was 7 times as active as a commercial Lindlar catalyst, while selectivity towards Z-stilbene was high. Our work also illustrated that highly selective Pd/Boehmite catalysts can be prepared by ultrasound-dispersion and microwave-reduction in water under hydrogen pressure without any surfactant.

Introduction

Hydrogenation reactions are performed in many areas of industry with hydrogen gas activated by nickel-, platinum- or palladium-based catalysts [1–3]. Palladium catalysts require the mildest of conditions and are the most widely used. In many cases, it is desired to obtain alkene from reduction of alkyne (*i.e.* to halt the reaction at the carbon-carbon double bond stage) – this class of reactions is termed as selective hydrogenation or semi-hydrogenation and it is widely used in the fine chemical industry, being one of the vital steps in the synthesis of vitamins (Vit. A, E, K), terpenes (linalool) and other products [2–4]. The main challenge in this process is to obtain the products of semi-hydrogenation in high yield (*i.e.* with high substrate conversion and selectivity), while minimizing the reaction duration, the number of reaction and separation steps such as protection of certain groups, separation of products or catalysts

2

from the product [5]. In addition, alkynes as impurities in feedstock are very strong poisons for Ziegler-Natta polymerization catalysts and should be converted into alkenes using semi-hydrogenation reactions [2,6,7]. Therefore, semi-hydrogenation reactions are important for the polyethylene and polypropylene production.

Traditional Pd catalysts for alkynes hydrogenation do not provide high selectivity in these processes and are usually modified with adsorbates such as quinoline, silver, lead or others, which increase selectivity while decreasing activity. Lindlar catalyst (Pd poisoned with lead and quinoline supported on $CaCO_3$) [8,9] was an industrial standard in fine chemistry for more than 50 years. However, there is a drive to develop new lead-free semi-hydrogenation catalysts for environmental reasons since lead is toxic [10]. Addressing the problem of toxicity and trying to increase performance, extensive research is being performed searching for other modifier metals such as Ga, Zn, and others [11–14]. However, bimetallic catalysts require complex synthesis routes; Pd-Ga intermetallic compounds were recently shown to be very oxygen sensitive even in carefully controlled air-free laboratory conditions [15]. On the other hand, monometallic Pd catalysts provide the highest catalytic activity and were demonstrated to provide very high selectivity [16] towards semi-hydrogenation. The hydrogenation of alkynes on solid Pd surfaces is a structure sensitive reaction, an important feature for the understanding of such catalytic processes [17,18]. The unselective hydrogenation proceeds on hydrogen-saturated β-hydride, whereas selective hydrogenation is only possible after decoupling bulk properties from the surface events [19] and only surface hydrogen from the gas phase is available to generate the alkene [20]. For this reason, effects of various supports, such as silica [21] and alumina [22] on the catalytic hydrogenation behavior have been extensively studied.

3

Non-conventional enabling technologies such as microwaves (MW) and ultrasound (US) foster process intensification and combine safer protocols and result in cost reduction and energy savings [23]. In comparison to conventional conductive heating, MW irradiation causes volumetric heating via the direct coupling of the electromagnetic field with polar solvents and catalysts in the reaction mixture. As a result, fast selective heating can be attained by irradiating polar materials in a MW field [24]. MW irradiation has proved to be a suitable energy source in catalyst preparation, because it allows one to generate nanoscale colloids and clusters of greater size and shape uniformity [25] - an important advantage for catalysis [26,27].

US enables the rapid dispersion of solids and facilitates the formation of porous materials and nanostructures [28]. Moreover, sonication can inhibit particle aggregation thanks to the intense implosion, which produces extreme chemical environments, caused by acoustic cavitation [29–31]. When a cavitation bubble collapses violently near a solid surface, the high-speed jets of liquid are driven into the surface of a particle [32]. Thus US is usually used to prepare catalytic materials and modify existing metal catalysts [33].

The excellent results on catalyst preparation by means of US- or MW-assisted protocols in previous studies [34] prompted us to explore new promising US- and MW-assisted synthetic routes for preparation of palladium-supported catalysts to be used in alkyne semi-hydrogenation [5,35]. Semi-hydrogenation of diphenylacetylene (DPA) is a traditional model reaction used to evaluate the behavior, mechanisms and kinetics of catalytic hydrogenation of internal alkynes [36,37]. In this piece of work we investigated how non-conventional preparation methods (US and MW) of lead-free Pd-catalysts may affect the kinetics of diphenylacetylene semi-hydrogenation.

4

Experimental section

Catalyst synthesis

Pd_{solv}/Boehmite and Pd_{solv}/CeO_2 catalysts were obtained by the US-assisted dispersion and reduction by solvent on boehmite and ceria supports, respectively. Palladium (II) acetate 20 mg ($Pd(OAc)_2$, Alfa-Aesar 99%) was suspended in 20 mL of ethylene glycol (Alfa-Aesar 99%) by sonication, obtaining orange salt suspension in the transparent solvent. The suspension was sonicated with a titanium immersion horn (21.1 kHz, 100-150 W) at about 100 °C and became a homogeneous black dispersion of Pd nanoparticles. The dispersion obtained was added dropwise to a stirring suspension of 1 g support in 10 mL of ethylene glycol. The mixture was stirred overnight at room temperature, the solid was filtered, washed with methanol and dried under vacuum.

Pd_{LV}/Boehmite catalyst was obtained by the reduction of $Pd(OAc)_2$ with Luviquat[TM] (hexadecyl(2-hydroxyethyl)dimethylammonium dihydrogen phosphate, (Sigma-Aldrich, 30% in H_2O). In to an aqueous solution of Luviquat[TM] (0.0365 mM), 30 mg of $Pd(OAc)_2$ was added followed by sonication in a cup-horn apparatus (cavitation tube, 19.9 kHz, 100 W) at 30 °C to obtain a pale orange suspension. The suspension was heated in a silicon oil bath at 80 °C and $Pd(OAc)_2$ was reduced with Luviquat[TM]. The obtained homogeneous black dispersion was added dropwise to a stirring suspension of 1.5 g of boehmite in 10 mL of water. The mixture was stirred overnight at room temperature. The solid was filtered, washed with water and dried under vacuum.

5

A one pot synthesis of Pd$_{LV-I}$/Boehmite catalyst was performed combining the dispersion with Luviquat^{TM} and deposition on to the support under sonication. The mixture of 30 mg of Pd(OAc)$_2$ and 1.5 g of boehmite were dispersed in 20 mL of aqueous solution of Luviquat^{TM} (0.0365 mM) in a cup-horn apparatus (cavitation tube, 19.9 kHz, 100 W) at 30 °C. Then the reduction and impregnation was carried out in an oil bath at 80 °C for 2 h. The mixture was stirred overnight at room temperature, and then the solid was filtered, washed with water and dried under vacuum.

A Luviquat^{TM}-free synthesis with the MW-assisted reduction with hydrogen produced Pd$_{US-MW}$ catalyst. 30 mg of Pd(OAc)$_2$ was suspended in H$_2$O (10 mL) and sonicated in a cup-horn apparatus (cavitation tube, 19.9 kHz, 100 W, Danacamerini sa.) at 30 °C to obtain a dispersion, which was then heated using MW under H$_2$ (10 bar, Sapio, grade 4.5) using a SynthWAVE reactor (MLS Gmbh, Milestone Srl) at 40 °C and 300 W MW power. After cooling the obtained black dispersion was added dropwise to a suspension of 1.5 g of boehmite in H$_2$O (10 mL). The mixture was stirred overnight at room temperature. Then the solid catalyst was filtered, washed with water and dried under vacuum.

Commercial Lindlar catalyst was purchased from Alfa-Aesar and used as a reference catalyst without the addition of quinoline.

Characterization

BET Measurements

Surface areas and pore distributions were measured by nitrogen physisorption using TriStar 3000 micromeritics surface area and porosity analyzer using standard multipoint BET analysis and BJH pore

6

distribution methods. All specimens were dried at 140 ^{o}C for 4 h in nitrogen flow before the measurements.

SEM Analysis

The catalysts were applied on a conductive carbon adhesive tape and coated with a thin layer of carbon to prevent charging. Scanning electron microscopy (SEM) study of the samples obtained was performed on the Zeiss EVO 60 instrument equipped with energy-dispersive X-ray spectrometer (EDX) Oxford Instruments Inca System 350 under the pressure of 10^{-2} Pa and electron acceleration voltage of 20 kV.

TEM Analysis

The catalyst samples were dispersed in ethanol under sonication and applied on polymer-coated copper grids. Transmission electron microscopy (TEM) study of the grids was performed using JEOL 2010 High Resolution Transmission Electron Microscope equipped with Oxford Instruments Energy Dispersive X-ray Microanalysis System.

ICP analysis

Palladium content was determined using the Perkin Elmer Optima 5300DV emission ICP instrument. The samples were dissolved in the solution of HF/ HCl/ HNO_3 in 1/1/3 ratio, heating at 200 ^{o}C for 10 min using microwave digestion system CEM MARS Xpress Plus. After cooling, the saturated aqueous solution of boric acid was added to complex excess HF, then the vessels were heated again at 180 ^{o}C for 10 min. The solutions were diluted with water and analyzed.

Catalyst Testing

The catalyst, 6.0 mg, was added in to a 12.0 mL of 56 mmol L^{-1} DPA (Alfa Aesar, 98%) solution in hexane (Sigma-Aldrich, 97%). Before hydrogenation, the reactor (Glass Vacuum Desiccator-containing 4 pieces of 48 mL PP cylindrical centrifuge tubes) was evacuated and filled nitrogen gas (Sapio, grade 6.0) to remove air followed by evacuation and filling with hydrogen gas (Sapio, grade 4.5). The reaction was performed at room temperature (23±1 °C) with stirring rates of 600 rpm and atmospheric hydrogen pressure (H_2 balloon). Aliquots (100 µL) of the solution were periodically extracted from the reaction system by airtight syringes, diluted with 900 µL cyclohexane (Alfa Aesar, 99.9%)and analyzed using a Agilent Technologies 6850 Network GC system equipped with 5973 Network Mass Selective Detector and the HP-5ms capillary column. Each hydrogenation process was performed in duplicate using the multi-tube reactor simultaneously. The concentrations difference in the duplicate runs deviated by less than 5%.

Results and Discussion

Effect of catalyst support with US-dispersion and reduction

The role of catalyst supports is a multifaceted issue that involves phenomena of chemical and physical catalyst-support interactions [38]. On the basic level, however, catalyst support acts as a matrix preventing sintering of the catalytically active Pd particles, so high surface area, thermostability are important characteristics of the catalyst support. Hence, alumina (along with carbon) is one of the widely used supports for hydrogenation catalysts. On the other hand, strong metal-support interactions

between Pd and the catalyst support such as cerium (IV) oxide were shown to enhance activity and selectivity of hydrogenation reactions [39,40].

Pd_{solv}/Boehmite and Pd_{solv}/CeO_2 catalysts were obtained reducing palladium (II) acetate with ethylene glycol at 100 ^{o}C in the presence of boehmite and ceria supports, respectively. Fig. 1 shows SEM microphotographs of the catalyst particles. Boehmite consists of non-uniform mainly spheroid particles from 1 to 100 μm in diameter (Fig. 1a). Ceria particles, on contrary, are uniform having the dimensions of approximately 50 μm (Fig. 1b).
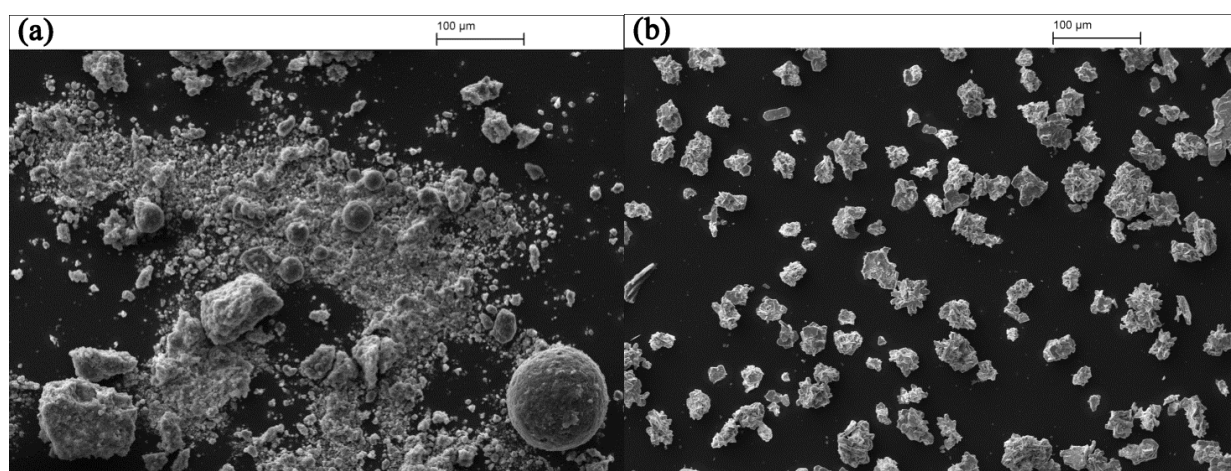

Fig. 1. SEM microphotographs of the (a) Pd_{solv}/Boehmite and (b) Pd_{solv}/CeO_2 catalyst particles.

Fig. 2 presents the nitrogen physisorption data of the catalysts obtained. Both of catalysts demonstrated type IV adsorption isotherms according to IUPAC classification, which are characteristic for many mesoporous sorbents [41]. However, the amount of adsorbed nitrogen on these catalysts was very different (Fig. 2a) as specific surface area of ceria-supported catalyst (Pd_{solv}/CeO_2) was almost two

9

orders of magnitude lower than that of boehmite-supported catalyst (Pd_{solv}/Boehmite), Table 1. Similarly, BJH desorption pore distribution (Fig. 2b) showed that ceria-supported catalyst (Pd_{solv}/CeO_2) was practically non-porous, while boehmite-supported catalyst (Pd_{solv}/Boehmite) was mesoporous. Hence, ceria particles had only external surface area available for the catalyst, while boehmite contained significant amount of mesopores that can be accessible for Pd nanoparticles.

Table 1. Pd content, textural properties and catalytic performance of the catalysts studied.

Catalyst	W_{Pd}[a]	S_{BET}	V_{pore}[b]	d_{pore}[c]	$d_{av.\ pore}$[d]	A_{init}[e]	S_{DPE}[f]
	(%)	($m^2\ g^{-1}$)	($cm^3\ g^{-1}$)	(nm)	(nm)	($mol\ g^{-1}Pd\ h^{-1}$)	(%)
Pd_{solv}/Boehmite	0.72	234	0.43	3.9	6.8	5.4	81.0
Pd_{solv}/CeO_2	1.33	3.6	0.02	3.2	12.9	3.0	81.7
Pd_{LV}/Boehmite	0.69	115	0.29	3.5	7.7	16.8	87.0
Pd_{LV-1}/Boehmite	0.78	115	0.29	3.5	6.7	18.6	88.0
Pd_{US-MW} /Boehmite	0.88	231	0.43	3.9	6.0	6.6	87.5
Lindlar	4.22	3.3	0.01	2.4	13.0	2.4	93.2

[a] Pd content in % mass; [b] BJH Desorption cumulative volume of pores between 1.7 nm and 300 nm diameter; [c] the most frequent BJH desorption pore diameter; [d] BJH desorption average pore diameter (4V/A); [e] initial activity of DPA consumption; [f] Z-1,2-Diphenylethene (Z-DPE) selectivity at the 90% DPA conversion.
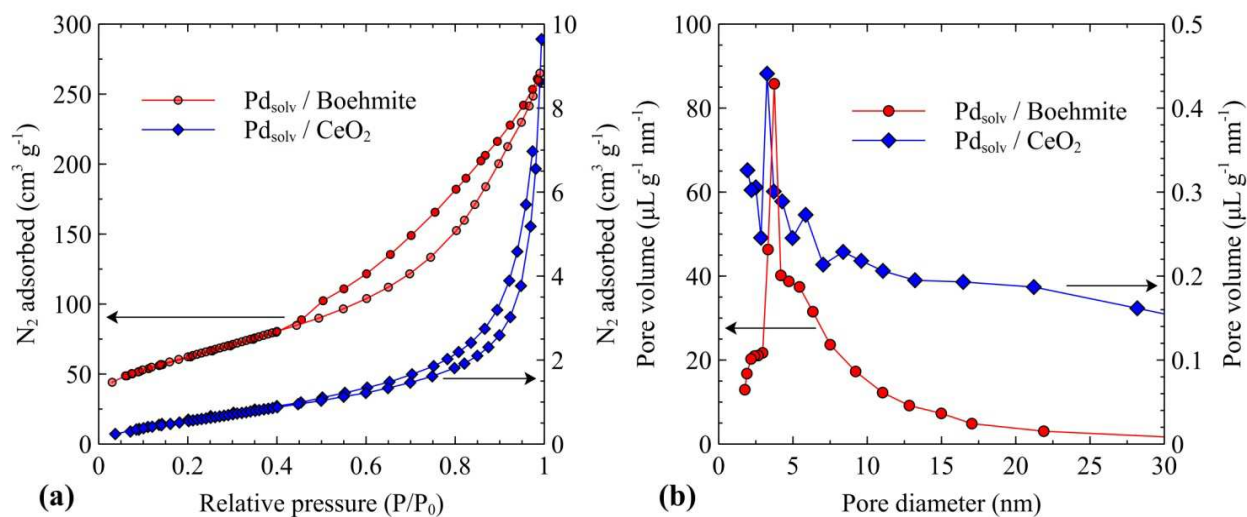
Fig. 2. (a) Nitrogen physisorption isotherms of Pd_{solv}/CeO_2 and $Pd_{solv}/Boehmite$ catalysts, (b) BJH desorption pore distribution.

TEM study of $Pd_{solv}/Boehmite$ catalyst demonstrated that Pd nanoparticles 20 ± 5 nm in diameter formed agglomerates on the surface of the boehmite catalyst support, as shown in Fig. 3. Ceria-supported catalyst Pd_{solv}/CeO_2 was also studied, but because cerium is heavier than palladium, the contrast was not enough to identify Pd nanoparticles. However, based on higher Pd content and much lower surface area of the ceria support, the diameter of the obtained nanoparticles in Pd_{solv}/CeO_2 was expected much higher than that in Pd_{solv} catalyst.
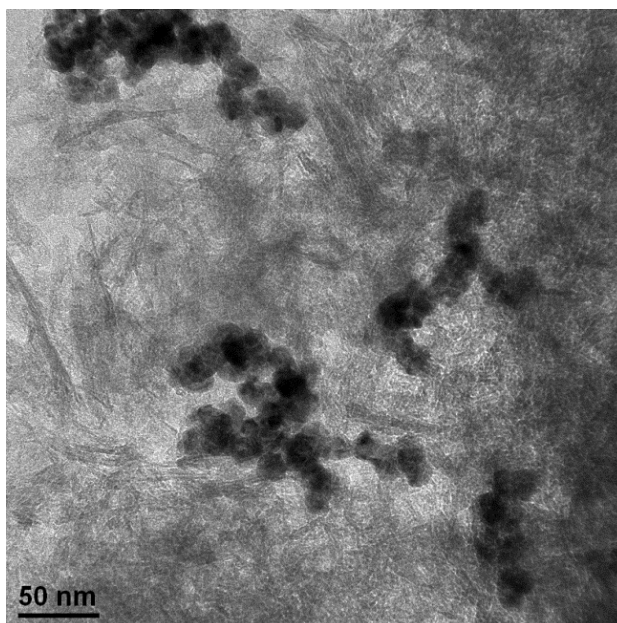
11

Fig. 3. TEM microphotograph of Pd$_{solv}$/Boehmite catalyst. EDX analysis confirmed that dark areas are Pd nanoparticles.

Fig. 4 shows concentration profiles of DPA hydrogenation on Pd$_{solv}$/CeO$_2$ and Pd$_{solv}$/Boehmite catalysts. The profiles are typical for Langmuir-Hinshelwood hydrogenation reactions with quasi-zero-order kinetics during the initial stages. Performance of the catalysts was very similar – full conversion of the same amount of DPA required approximately 300 min with the highest *Z*-DPE selectivity of about 75%. However, considering that the Pd content in Pd$_{solv}$/CeO$_2$ catalyst is twice higher (Table 1), Pd$_{solv}$/Boehmite catalyst was more active per mole of Pd.
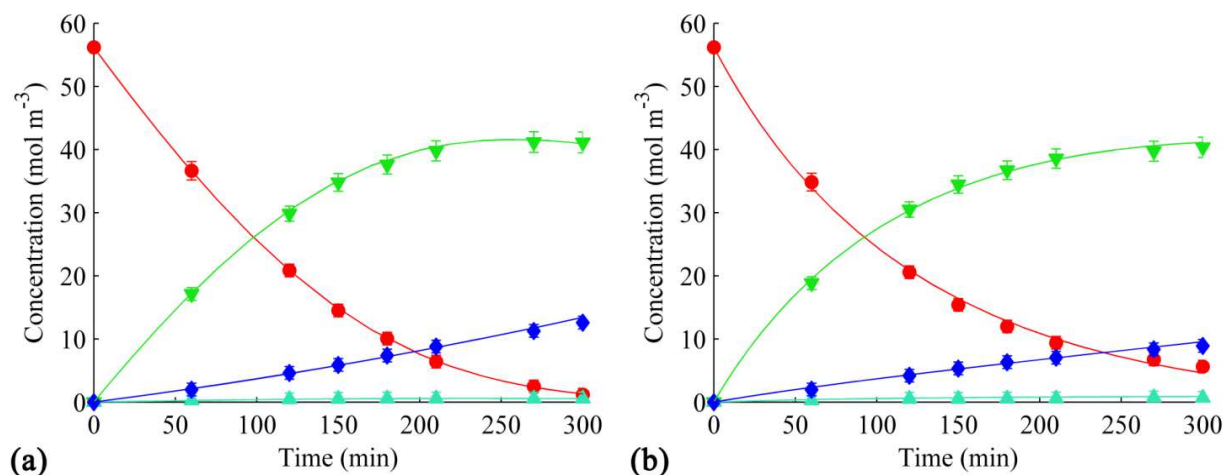
12

Fig. 4. Concentration profile during hydrogenation of DPA on (a) Pd$_{solv}$/Boehmite and (b) Pd$_{solv}$/CeO$_2$ catalysts: concentration of (●) DPA, (▼) Z-DPE, (▲) E-DPE, (♦) diphenylethane.

Effect of reducing agent and surfactant with US-dispersion

With the aim to further increase activity and improve the selectivity towards *Z*-DPE, Pd$_{LV}$/Boehmite catalyst was obtained using Luviquat^{TM} that acts both as a reducing and a capping agent [42–44]. Fig. 5 shows a representative TEM image of Pd$_{LV}$/Boehmite catalyst with Pd nanoparticles 3.0±1.1 nm. In comparison to the surfactant-free Pd$_{solv}$/Boehmite catalyst, the diameter of Pd nanoparticles significantly decreased and the particles were uniformly distributed on the catalyst surface.
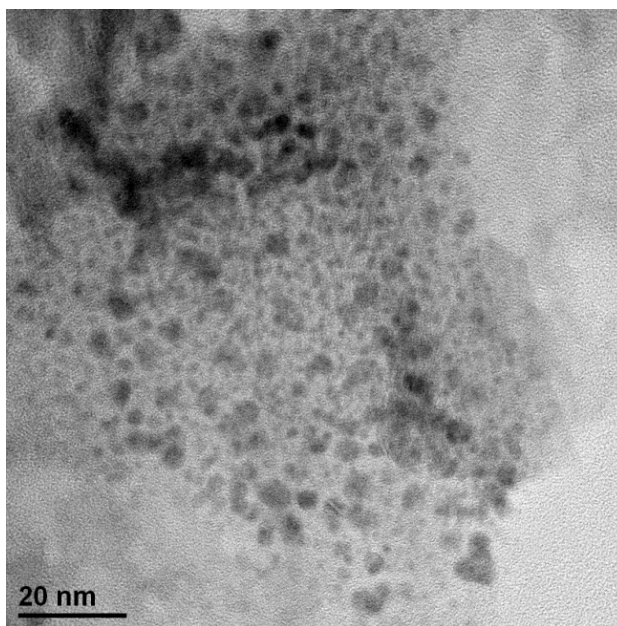
Fig. 5. TEM microphotograph of Pd$_{LV}$/Boehmite catalyst.

Interestingly, total BET surface area had twofold decrease in comparison to the surfactant-free Pd$_{solv}$/Boehmite catalyst (Table 1). Pore distribution had also changed, as shown in Fig. 6 – the proportion of the pores smaller than 2 nm (micropores) and the pores larger than 4 nm decreased. These effects can be attributed to the strong adsorption of the surfactant molecules in the catalyst pores or to restructuring of the boehmite structure directed by the surfactant molecules [45,46].
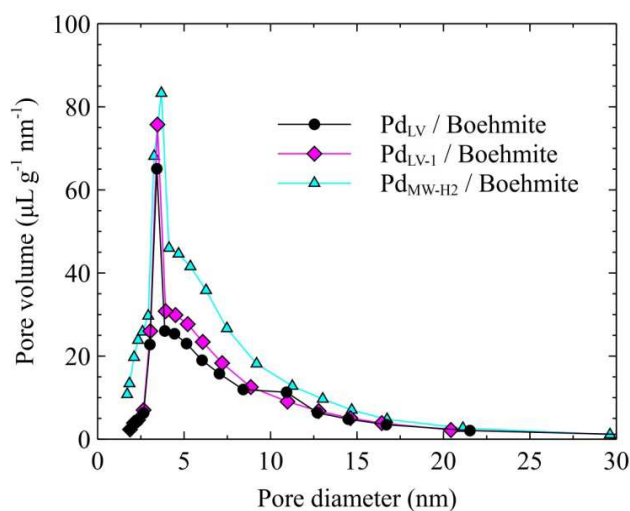
14

Fig. 6. BJH desorption pore distribution for Pd$_{LV}$/Boehmite, Pd$_{LV-1}$/Boehmite, Pd$_{US-MW}$/Boehmite catalysts.

As expected, Pd$_{LV}$/Boehmite catalyst demonstrated much higher activity in comparison to Pd$_{solv}$/Boehmite catalyst, although Pd content in Pd$_{LV}$/Boehmite was much lower than that in Pd$_{solv}$/Boehmite (Table 1) – full conversion of DPA took place within 80 minutes, as shown in Fig. 7. So drastic increase in activity agreed with the TEM data, because much smaller Pd nanoparticles found in Pd$_{LV}$/Boehmite catalyst, exposed more active surface Pd sites. Moreover, *Z*-DPE selectivity of Pd$_{LV}$/Boehmite catalyst at full DPA conversion increased to 87% from 81% for Pd$_{solv}$/Boehmite catalyst. This effect can also be explained considering smaller Pd particles. As the diameter of the nanoparticles decreases, higher fraction of Pd atoms occupies step sites [47,48], while these step sites provide higher alkene selectivity due to the suppression of undesirable full hydrogenation reactions [49].
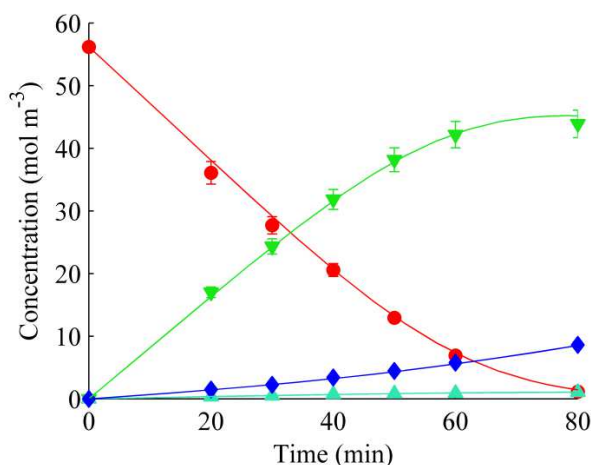
15

Fig. 7. Concentration profile during DPA hydrogenation on Pd$_{LV}$/Boehmite catalyst: concentration of (●) DPA, (▼) Z-DPE, (▲) E- DPE, (♦) diphenylethane.

Effect of ultrasound in a one-pot procedure

To simplify the preparation process and improve the activity and selectivity of Z-DPE further, Pd$_{LV-1}$/Boehmite catalyst was prepared using one-pot method, performing dispersion of Pd(OAc)$_2$ and boehmite using sonication simultaneously in the presence of Luviquat^{TM}. Textural properties of the catalyst obtained were identical to that of Pd$_{LV}$/Boehmite catalyst (Table 1 and Fig. 6). However, higher Pd content in Pd$_{LV-1}$/Boehmite shows that sonication facilitated Pd deposition on boehmite (Table 1).

According to TEM data, the average diameter of Pd nanoparticles obtained was 2.4±0.7 nm, *i.e.* smaller than that of Pd$_{LV}$/Boehmite catalyst even despite of higher Pd loading, likely, due to stabilization of the nanoparticles with Luviquat^{TM} and effect of sonication in one-pot procedure.
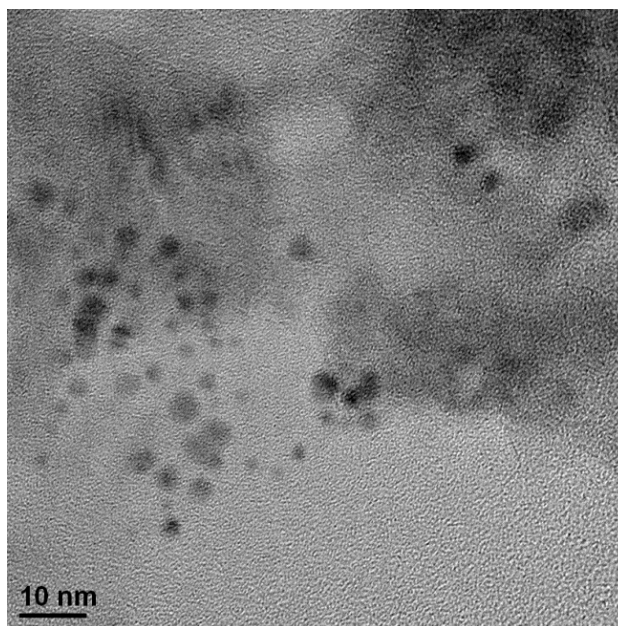
16

Fig. 8. TEM microphotograph of Pd$_{LV-1}$/Boehmite catalyst.

Concentration profiles of DPA hydrogenation shown in Fig. 9 correlate with the decreased Pd particle size – activity and selectivity of the catalyst were higher (Table 1). These data are in excellent agreement with the smaller diameter of Pd nanoparticles observed by TEM due to higher selectivity of edge sites towards internal Z-alkene formation [49].
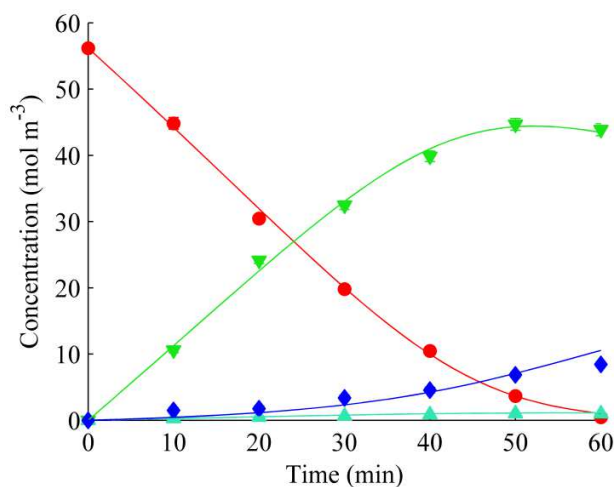
17

Fig. 9. Concentration profile during hydrogenation of DPA on Pd$_{LV-1}$/Boehmite catalyst: concentration of (●) DPA, (▼) *Z*-DPE, (▲) E- DPE, (♦) diphenylethane.

Effect US-assisted dispersion and MW-assisted reduction for Pd/Boehmite preparation

As the diameter of Pd nanoparticles decreased on ultrasonic synthesis of Pd$_{LV-1}$/Boehmite catalyst, a similar, but surfactant-free synthesis was tried. Catalyst Pd$_{US-MW}$/Boehmite was obtained through dispersion of palladium(II) acetate in water by sonication, and then reduction in the atmosphere of hydrogen with MW heating. The catalyst demonstrated identical surface and porosity properties as Pd$_{solv}$/Boehmite catalyst obtained with the reduction-by-solvent of palladium(II) acetate (Table 1). However, Pd content of Pd$_{US-MW}$/Boehmite was higher than that of Pd$_{solv}$/Boehmite catalyst, likely, due to enhanced Pd reduction by US and MW treatment. Pore diameter distribution of Pd$_{US-MW}$/Boehmite and Pd$_{solv}$/Boehmite catalysts were also identical in comparison Fig. 6, *i.e.* MW treatment did not affect the properties of the boehmite support.

18

Fig. 10 shows that Pd$_{US-MW}$/Boehmite catalyst contains Pd nanoparticles that form clusters about 100 nm in diameter. The formation of the agglomerates demonstrates that US-assisted dispersion and MW-assisted reduction cannot prevent agglomeration of the forming nanoparticles without a capping agent.
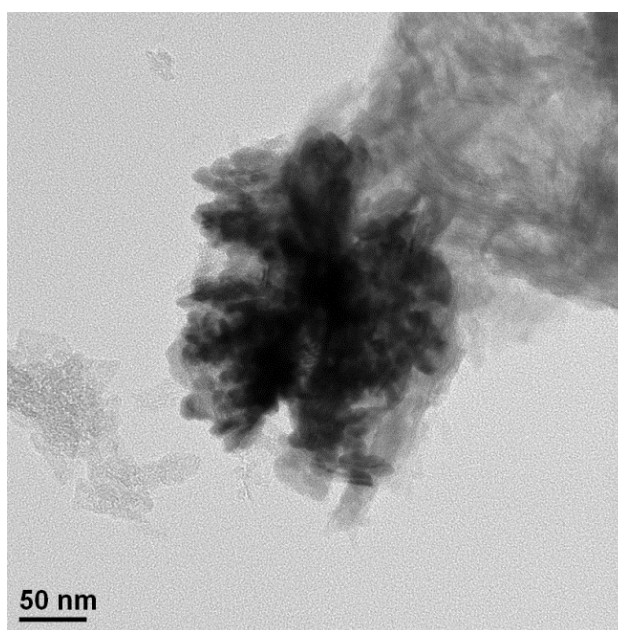

50 nm

Fig. 10. TEM microphotograph of Pd$_{US-MW}$/Boehmite catalyst.

Fig. 11 shows concentration profiles of DPA hydrogenation on Pd$_{US-MW}$/Boehmite catalyst. US-assisted dispersion and MW-assisted reduction were shown to enhance activity and selectivity of *Z*-DPE without a capping agent in comparison to Pd$_{solv}$/Boehmite catalyst (Fig.4a). Full DPA conversion for the same amount of DPA reduced from 300 to 170 min for Pd$_{US-MW}$/Boehmite catalyst in comparison to Pd$_{solv}$/Boehmite, while in the DPA conversion range of 85-95%, *Z*-DPE selectivity was about 5% higher

19

in comparison to Pd_{solv}/Boehmite. However, Z-DPE selectivity was very close for Pd_{US-MW}/Boehmite, Pd_{LV-1}/Boehmite, Pd_{LV}/Boehmite catalysts, so it may be concluded that individual Pd nanoparticles formed during MW-US-assisted synthesis were very similar to that obtained using the capping agent. In the case of Pd_{LV-1}/Boehmite, Pd_{LV}/Boehmite catalysts, small Pd nuclei formed were stabilized by the capping agent giving rise to small Pd nanoparticles. In case of Pd_{US-MW}/Boehmite catalyst, quick and uniform heating using MW lead to simultaneous nucleation of Pd nanoparticles. However, due to the lack of a capping agent, the formed nanoparticles quickly agglomerated (Fig. 10), still retaining the large number of surface step sites which can explain high DPE selectivity.
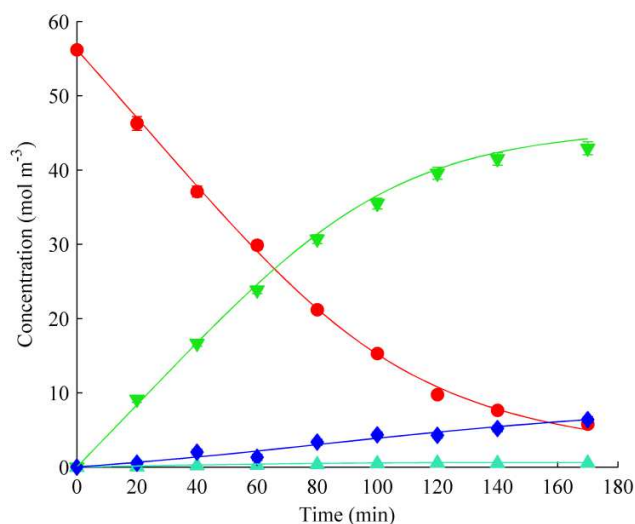

Fig. 11. Concentration profile during hydrogenation of DPA on Pd_{US-MW}/Boehmite catalyst: concentration of (●) DPA, (▼) Z-DPE, (▲) E- DPE, (♦) diphenylethane.

Kinetic modeling – comparison with Lindlar catalyst

Effect of mass transfer on reaction rates

The Weisz-Prater criterion is widely used to ensure that a catalytic reaction is not diffusion-limited. If the Weisz-Prater number is below 6 for zero-order reactions for every major reaction and product component, it proves that the reaction is not diffusion-limited [50,51]. The Weisz-Prater number (equation 1) is calculated using $\Re$ (effective reaction rate [mol m^{-3} s^{-1}]), R_p (radius of the catalyst particle [m]), C and D_{eff} (concentration [mol m^{-3}] and effective diffusion coefficient [m^2 s^{-1}] of a reactant or a product).

$$N_{W-P} = \frac{\Re \, R_p^2}{C \, D_{eff}} \qquad (1)$$

In order to ensure that mass transfer limitations did not apply for all catalytic systems studied, upper boundary estimation of the Weisz-Prater number (equation 1) was performed using the largest possible values for $\Re$ and R_P - 0.02 mol m^{-3} s^{-1} observed for Pd$_{LV-1}$/Boehmite catalyst and $R_p = 10^{-4}$ m, the largest catalyst particle size observed by SEM study (Fig. 1b).

The bulk diffusion coefficients for hydrogen and DPA were estimated using the methods described in details by Vannice [51]. The resulting coefficients and the Weisz-Prater numbers for these molecules presented were 0.004 for hydrogen and 0.036 for DPA, several orders of magnitude lower than the boundary value of 6, hence kinetic modeling was carried out considering only intrinsic kinetics rather than mass transfer phenomena.

Kinetic Modeling

Hydrogenation kinetics of semi-hydrogenations are modeled by considering the sequential reductions of alkyne to alkene, followed by alkene to alkane hydrogenation. In addition, a number of authors have also considered and modeled a direct route of full hydrogenation of alkyne to alkane which is independent of the sequential hydrogenation sequence and may occur even at low alkene concentrations [13,52–54]. We believe that this is mechanistically unlikely, however to ensure that a possible hydrogenation pathway is not ignored and to allow direct comparison with previous works we have also included a term for the direct hydrogenation from the alkyne to alkane in our kinetic model. In the case of DPA, alkenes can be formed in either their Z- or E- geometries, hence, the full reaction scheme contains of 5 possible stages, Scheme 1.
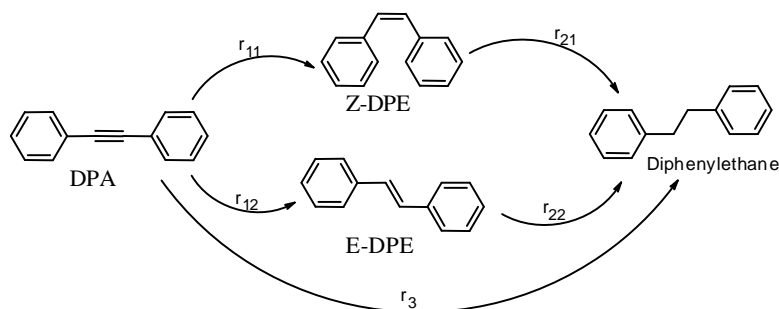
Scheme 1 DPA hydrogenation reactions.

Each of the stages is, in turn, described by the Langmuir-Hinshelwood mechanism that consists of quasi-equilibrium adsorption of hydrogen and organic species, and the rate-limiting step of the addition of the hydrogen species followed by desorption [55,56]. Full derivation of the model is presented in the

22

Supporting Information. Briefly, the model consists of a system of 5 ordinary differential equations which includes 7 parameters: 5 apparent rate constants (Scheme 1) and 2 relative adsorption constants $Q_1=K_{DPE}/K_{DPA}$ and $Q_2=K_{Diphenylethane}/K_{DPA}$. The system of differential equations was integrated using a program written in Matlab with a 4th-order Runge-Kutta method and the model parameters were optimized using the Levenberg–Marquardt algorithm to fit the experimental data. Objective function for minimization was calculated as statistic weighted squared residual, equation (2), where $C_{exp, i}$, $C_{modelled, i}$ are experimental and calculated concentrations of components respectively, and w_i statistical weights calculated taking experimental uncertainties ($\sigma_{experimental,i}$) of 2% of the experimental concentration or 0.3 mol m^{-3}, whichever is larger.

$$S = \sum w_i (C_{exp,i} - C_{modelled,i})^2, \; w_i = 1/\sigma^2_{experimental,i} \qquad (2)$$

Confidence intervals of the model parameters were determined using the Monte-Carlo method [57] – 500 sets of initial data normally distributed with the standard deviations ($\sigma_{experimental,i}$) were generated and kinetic parameters were obtained fitting the experimental data. Resulting uncertainties were calculated as 90% confidence intervals.

Comparison of Pd$_{LV-1}$/Boehmite with Lindlar catalyst

Lindlar catalyst has been an industrial standard for semi-hydrogenation reactions for more than 50 years, so Pd$_{LV-1}$/Boehmite catalyst was compared with it. In order to get quantitative information on the reaction stages, DPA was hydrogenated on Lindlar catalyst and kinetic modeling using the relative

23

constants Langmuir-Hinshelwood model was performed. The model was in excellent agreement with the experimental data for Lindlar and Pd_{LV-1}/Boehmite catalysts - lines in Fig. 9, Fig. 12 show modeled concentration profiles, while the dots - experimental values.
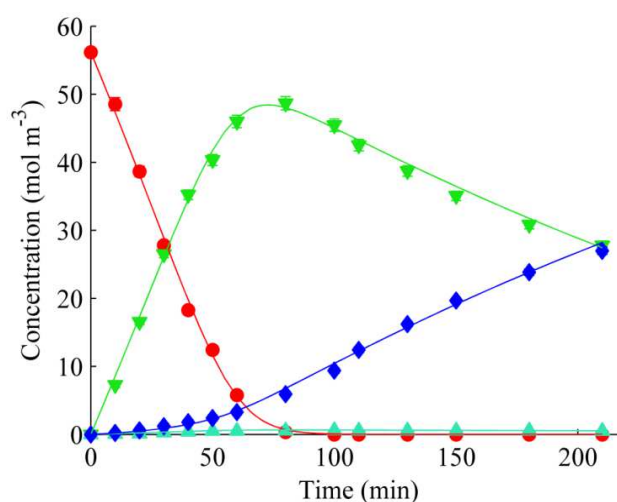

Fig. 12. Concentration profile during DPA hydrogenation on Lindlar catalyst: concentration of (●) DPA, (▼) Z-DPE, (▲) E- DPE, (♦) diphenylethane.

Table 2 presents the obtained model parameters. Apparent rate constant k^*_{11} of DPA hydrogenation into Z-DPE shows that Pd_{LV-1}/Boehmite provided 1.3 times faster DPA hydrogenation rate in comparison to Lindlar catalyst per unit of the catalyst mass. Considering more than 5-fold higher Pd content in Lindlar catalyst, Pd_{LV-1}/Boehmite catalyst demonstrated significant increase in activity. However, other rate constant ratios were about 2.5, which means that all undesired reactions such as full hydrogenation and Z-E isomerisation were faster (even in relative terms) on Pd_{LV-1}/Boehmite catalyst. Rate constant k^*_{22} of E-DPE hydrogenation demonstrated very wide confidence intervals, because of high errors of E-DPE

24

determination due to its very low concentration in the reaction mixture. Relative adsorption constants Q_1 which show poisoning of the catalytic surface with alkene were similar for both systems, while constant Q_2 is higher for Pd_{LV-1}/Boehmite catalyst, *i.e.* alkane molecules stronger adsorb on the Pd surface rather than Pb-doped Pd. As a result, maximum alkene selectivity of Lindlar catalyst is higher than that of Pd_{LV-1}/Boehmite catalyst (91 vs. 85% at 95% DPA conversion). Hence, the data demonstrate that lead in Lindlar catalyst does not significantly change the ratio of alkene to alkyne adsorption constants, while possibly changing the absolute values of the constants. The most important role of lead is usually explained by the significant change in the adsorption energies of intermediate reaction species [58]. However, a very similar relative adsorption constants obtained in the current study indicate that this thermodynamic explanation does not apply for the studied DPA hydrogenation reaction. On contrary, lower apparent reaction rates observed for Lindlar catalyst imply that the active site poisoning plays more important role in enhancing the semi-hydrogenation selectivity [49].

Table 2. The comparison of the kinetic parameters for Lindlar and Pd_{LV-1}/Boehmite catalysts. 90% confidence intervals are obtained using the Monte-Carlo error analysis [57].

Parameter[a]	Pd_{LV-1}/Boehmite	Lindlar	Ratio[b]
k_{11}^{*} $(s^{-1}\ g_{cat}^{-1})$	174±5	131±3	1.33±0.07
k_{21}^{*} $(s^{-1}\ g_{cat}^{-1})$	11±1	4.3±0.5	2.64±0.62
k_{3}^{*} $(s^{-1}\ g_{cat}^{-1})$	5.4±1.7	2.9±1.1	2.42±1.47
k_{12}^{*} $(s^{-1}\ g_{cat}^{-1})$	4.0±0.3	1.7±0.2	2.37±0.42
k_{22}^{*} $(s^{-1}\ g_{cat}^{-1})$	4.3±1.3	1.8±1.7	14.6±13.75
$Q_1{}^{c}$	0.39±0.02	0.37±0.02	1.07±0.13
$Q_2{}^{c}$	0.35±0.03	0.26±0.05	1.42±0.39

[a] Apparent rate constant correspond to Scheme 1; [b] the ratio of the corresponding kinetic parameters of Pd_{LV-1}/Boehmite and Lindlar catalysts; [c] Q_1 and Q_2 are relative adsorption constants of alkene to alkyne and alkane to alkyne, respectively. See Supporting information for a full model description.

Conclusions

The effect of sonication, the capping agent (Luviquat^{TM}) and the reduction by microwave heating on the Pd catalyst preparation was studied. The combination of the capping agent and sonication allowed us to obtain monodisperse 2.4±0.7 nm Pd nanoparticles supported on boehmite during a one-pot synthesis. The catalyst was about 7 times as active as a commercial Lindlar catalyst per unit of Pd mass taken, while only 6% (at 95% conversion) less selective towards semi-hydrogenation. Kinetic modeling performed indicates that the improved selectivity of Lindlar catalyst is attributed to the active site poisoning, rather than thermodynamic effects.

Microwave-assisted synthesis of Pd$_{US-MW}$/Boehmite catalyst demonstrated that although large agglomerates of Pd nanoparticles were formed, semi-hydrogenation selectivity was significantly higher than that of conventionally-heated Pd$_{solv}$/Boehmite catalyst. This difference suggests that the catalyst contains a lot of step Pd sites, like the catalysts containing smaller nanoparticles.

Acknowledgements

References

[1]   G. W. Watson, R. P. K. Wells, D. J. Willock, G. J. Hutchings, *J. Phys. Chem. B* **2001**, *105*, 4889–4894.

[2]   Á. Molnár, A. Sárkány, M. Varga, *J. Mol. Catal. A Chem.* **2001**, *173*, 185–221.

[3]   W. Bonrath, J. Medlock, J. Schutz, B. Wüstenberg, T. Netscher, *Hydrogenation in the Vitamins and Fine Chemicals Industry – An Overview, In: I. Karame (Ed.) Hydrogenation, InTech, Rijeka, 2012, pp. 69-90.*

[4]   M. Eggersdorfer, D. Laudert, U. Létinois, T. McClymont, J. Medlock, T. Netscher, W. Bonrath, *Angew. Chem. Int. Ed. Engl.* **2012**, *51*, 12960–12990.

[5]   V. Hessel, G. Cravotto, P. Fitzpatrick, B. S. Patil, J. Lang, W. Bonrath, *Chem. Eng. Process. Process Intensif.* **2013**, *71*, 19–30.

[6]   A. N. R. Bos, K. R. Westerterp, *Chem. Eng. Process. Process Intensif.* **1993**, *32*, 1–7.

[7]   J. Gislason, W. Xia, H. Sellers, *J. Phys. Chem. A* **2002**, *106*, 767–774.

[8]   H. Lindlar, *Helv. Chim. Acta* **1952**, *35*, 446–450.

[9]   H. Lindlar, R. Dubuis, *Org. Synth.* **1966**, *46*, 88–89.

[10]   L. N. Protasova, E. V. Rebrov, K. L. Choy, S. Y. Pung, V. Engels, M. Cabaj, A. E. H. Wheatley, J. C. Schouten, *Catal. Sci. Technol.* **2011**, *1*, 768–77.

[11]   J. Rajaram, A. P. S. Narula, H. P. S. Chawla, S. Dev, *Tetrahedron* **1983**, *39*, 2315–2322.

28

[12]   J. Osswald, K. Kovnir, M. Armbrüster, R. Giedigkeit, R. E. Jentoft, U. Wild, Y. Grin, R. Schlögl, *J. Catal.* **2008**, *258*, 219–227.

[13]   E. V Rebrov, E. A. Klinger, A. Berenguer-Murcia, E. M. Sulman, J. C. Schouten, *Org. Process Res. Dev.* **2009**, *13*, 991–998.

[14]   N. López, C. Vargas-Fuentes, *Chem. Commun.* **2012**, *48*, 1379–1391.

[15]   G. Wowsnick, D. Teschner, M. Armbrüster, I. Kasatkin, F. Girgsdies, Y. Grin, R. Schlögl, M. Behrens, *J. Catal.* **2014**, *309*, 221–230.

[16]   S. Dominguez-Dominguez, A. Berenguer-Murcia, A. Linares-Solano, D. Cazorla-Amoros, *J. Catal.* **2008**, *257*, 87–95.

[17]   J. G. Ulan, W. F. Maier, D. A. Smith, *J. Org. Chem.* **1987**, *52*, 3132–3142.

[18]   P. W. Albers, K. Möbus, C. D. Frost, S. F. Parker, *J. Phys. Chem. C* **2011**, *115*, 24485–24493.

[19]   D. Teschner, J. Borsodi, A. Wootsch, Z. Révay, M. Hävecker, A. Knop-Gericke, S. D. Jackson, R. Schlögl, *Science* **2008**, *320*, 86–89.

[20]   D. Teschner, E. Vass, M. Havecker, S. Zafeiratos, P. Schnorch, H. Sauer, A. Knopgericke, R. Schlogl, M. Chamam, A. Wootsch, *J. Catal.* **2006**, *242*, 26–37.

[21]   T. A. Nijhuis, G. van Koten, J. A. Moulijn, *Appl. Catal. A Gen.* **2003**, *238*, 259–271.

[22]   D. R. Kennedy, G. Webb, S. D. Jackson, D. Lennon, *Appl. Catal. A Gen.* **2004**, *259*, 109–120.

[23]   G. Cravotto, S. Tagliapietra, M. Caporaso, D. Garella, E. Borretto, A. Stilo, *Chem. Heterocycl. Compd.* **2013**, *49*, 811–826.

[24]   C. O. Kappe, *Angew. Chem. Int. Ed. Engl.* **2004**, *43*, 6250–6284.

[25]   W. Tu, H. Liu, *Chem. Mater.* **2000**, *12*, 564–567.

[26]   T. S. Ahmadi, Z. L. Wang, T. C. Green, A. Henglein, M. A. El-Sayed, *Science* **1996**, *272*, 1924–1925.

[27]   W. Bonrath, *Ultrason. Sonochem.* **2005**, *12*, 103–106.

[28]   P. Cintas, J.-L. Luche, *Green Chem.* **1999**, *1*, 115–125.

[29]   K. S. Suslick, *Science* **1990**, *247*, 1439–1445.

[30]   N. A. Dhas, A. Gedanken, *Chem. Mater.* **1997**, *9*, 3144–3154.

[31]   T. Prozorov, R. Prozorov, K. S. Suslick, *J. Am. Chem. Soc.* **2004**, *126*, 13890–13891.

[32]   B. Toukoniitty, J.-P. Mikkola, D. Y. Murzin, T. Salmi, *Appl. Catal. A Gen.* **2005**, *279*, 1–22.

[33]   J. H. Bang, K. S. Suslick, *Adv. Mater.* **2010**, *22*, 1039–1059.

[34]   Z. Wu, E. Borretto, J. Medlock, W. Bonrath, G. Cravotto, *ChemCatChem* **2014**, *6*, 2762–2783.

[35]   G. Cravotto, W. Bonrath, S. Tagliapietra, C. Speranza, E. C. Gaudino, A. Barge, *Chem. Eng. Process. Process Intensif.* **2010**, *49*, 930–935.

[36] R. D. Adams, T. S. Barnard, Z. Li, W. Wu, J. Yamamoto, *J. Am. Chem. Soc.* **1994**, *116*, 9103–9113.

[37] J. A. Cabeza, J. M. Fernandez-Colinas, A. Llamazares, V. Riera, S. Garcia-Granda, J. F. Van der Maelen, *Organometallics* **1994**, *13*, 4352–4359.

[38] J. A. Schwarz, C. Contescu, A. Contescu, *Chem. Rev.* **1995**, *95*, 477–510.

[39] R. S. Monteiro, F. B. Noronha, L. C. Dieguez, M. Schmal, *Appl. Catal. A Gen.* **1995**, *131*, 89–106.

[40] G. Vilé, B. Bridier, J. Wichert, J. Pérez-Ramírez, *Angew. Chemie* **2012**, *51*, 8620–8623.

[41] K. S. W. Sing, D. H. Everett, R. A. W. Haul, L. Moscou, R. A. Pierotti, J. Rouqerol, T. Siemieniewska, *Pure Appl. Chem.* **1985**, *57*, 603–619.

[42] E. Boymans, S. Boland, P. T. Witte, C. Müller, D. Vogt, *ChemCatChem* **2013**, *5*, 431–434.

[43] P. T. Witte, M. de Groen, R. M. de Rooij, P. Bakermans, H. G. Donkervoort, P. H. Berben, J. W. Geus, *Stud. Surf. Sci. Catal.* **2010**, *175*, 135–143.

[44] P. T. Witte, *Process for the Preparation of an Aqueous Colloidal Precious Metal Suspension*, **2009**, WO2009096783 A1.

[45] H. C. Lee, H. J. Kim, C. H. Rhee, K. H. Lee, J. S. Lee, S. H. Chung, *Microporous Mesoporous Mater.* **2005**, *79*, 61–68.

[46] O. Weichold, T. Dederichs, M. Möller, *J. Colloid Interface Sci.* **2007**, *306*, 300–306.

[47] D. Y. Murzin, *J. Catal.* **2010**, *276*, 85–91.

31

[48] D. Y. Murzin, *Chem. Eng. Sci.* **2009**, *64*, 1046–1052.

[49] J. A. Anderson, J. Mellor, R. K. P. K. Wells, *J. Catal.* **2009**, *261*, 208–216.

[50] P. B. Weisz, C. D. Prater, *Adv. Catal.* **1954**, *6*, 143–196.

[51] M. A. Vannice, *Kinetics of Catalytic Reactions*, Springer Science+Business Media, New York, **2005, pp. 61-77.**

[52] A. S. Al-Ammar, G. Webb, *J. Chem. Soc. Faraday Trans.* **1978**, *74*, 195-205.

[53] G. F. Berndt, S. J. Thomson, G. Webb, *J. Chem. Soc. Faraday Trans.* **1983**, *79*, 195–207.

[54] M. Crespo-Quesada, A. Yarulin, M. Jin, Y. Xia, L. Kiwi-Minsker, *J. Am. Chem. Soc.* **2011**, *133*, 12787–94.

[55] U. K. Singh, M. A. Vannice, *J. Catal.* **2000**, *191*, 165–180.

[56] D. Duca, L. F. Liotta, G. Deganello, *J. Catal.* **1995**, *154*, 69–79.

[57] J. S. Alper, R. I. Gelb, *J. Phys. Chem.* **1990**, *94*, 4747–4751.

[58] M. García-Mota, J. Gómez-Díaz, G. Novell-Leruth, C. Vargas-Fuentes, L. Bellarosa, B. Bridier, J. Pérez-Ramírez, N. López, *Theor. Chem. Acc.* **2010**, *128*, 663–673.